

On the Cosmic Variance of the Merger Rate Density of Binary Neutron Stars

ZHIWEI CHEN,^{1,2} YOUJUN LU,^{1,2} JIE WANG,^{1,2} ZHEN JIANG,³ QINGBO CHU,^{1,2} AND XIANGHAO MA^{1,2}

¹*National Astronomical Observatories, Chinese Academy of Sciences, 20A Datun Road, Beijing 100101, China*

²*School of Astronomy and Space Sciences, University of Chinese Academy of Sciences, 19A Yuquan Road, Beijing 100049, China*

³*Department of Astronomy, Tsinghua University, Beijing 100084, China*

ABSTRACT

The cosmic variance on the star formation history may lead to bias to the merger rate density estimation of binary neutron star (BNS) mergers by the compact binary population synthesis. In this paper, we take the advantage of the large boxsize of the Millennium Simulation combined with the semi-analytic galaxy formation model GABE, and the parameterized population binary star evolution (BSE) model to examine how much effect will the cosmic variance introduce on the estimation of merger rate density of BNS mergers. We find that for sub-box size of 100Mpc and 200Mpc, the variance of merger rate density $\sigma_{\text{R}}/\text{R}$ at different redshift is about 23% – 35% and 13% – 20% respectively. On one hand, as for the variance of the detection rate on BNS mergers with current LIGO-Virgo-KAGRA (LVK) detector network, this value is very small $\lesssim 10\%$, which indicates ignoring the cosmic variance is reasonable for estimating the merger rate density from current LVK observation. On the other hand, with next-generation gravitational wave detectors, it is possible to localize BNS mergers within sub-boxes possessing length of 40Mpc for source redshift $z_s < 0.2$. In such a small box, the cosmic variance of the merger rate density is significant, i.e., the value of $\sigma_{\text{R}}/\text{R}$ is about $\sim 55\%$. This hints that estimating the merger rate density of BNS in different sky areas may provide useful information on the cosmic variance.

Keywords: Gravitational wave astronomy (675) — Gravitational wave sources (677) — Galaxies (573)

1. INTRODUCTION

The first detection of gravitational wave (GW) emitted by the binary neutron star (BNS) merger GW170817 and its electromagnetic (**EM**) counterpart signals marks the beginning of a new era of multi-messenger astronomy (e.g., Abbott et al. 2017a,b; Coulter et al. 2017; Pian et al. 2017; Dobie et al. 2018; Coughlin et al. 2019; Abbott et al. 2019a). The associated EM counterpart can provide significant information on the physical properties of BNS mergers, for example, the tidal deformability and the equation of state constrained from the GW, afterglow, and kilonova signals (e.g., Gottlieb et al. 2018; Xie et al. 2018). Moreover, with the redshift measurement of the EM counterpart and luminosity distance measurement from the GW signal, BNS mergers can

be viewed as excellent standard sirens to constrain the cosmological parameters. For example, the Hubble constant can be constrained to a precision of $\sim 10\%$ by the data of GW170817, GRB170817A, and AT 2017gfo (The LIGO Scientific Collaboration et al. 2021). With the development of ground-based GW detectors, it is anticipated to observe many more GW170817-like objects in the near future, which may constrain H_0 to $\sim 1\%$ precision.

It is crucial to estimate the evolution of merger rate density of BNS mergers. The merger rate density of the BNS mergers are dependent on the detailed physics embedded in the binary evolution procedure, including the common envelope ejection, Roche lobe mass transfer process, and the production of natal kick (e.g., Chu et al. 2022). For example, if the natal kick is large enough, the BNS may not form at the end of its progenitor life, which may decrease the merger rate density of BNS mergers significantly. Another important recipe is the star-formation-rate (SFR) evolution of galaxies in

our universe. The lower SFR will result in less compact binary formation and thus lower the merger rate density. Therefore, it is possible to constrain such important physical recipes by comparing the measurement to the results given by compact binary population synthesis.

Cosmological numerical simulation has been widely used to estimate the merger rate density and predict the performance of ground-based GW detectors of double compact objects. However, almost all the works done so far just simply take an average (global) of the resulted merger rate density in the full box of the hydrodynamical simulations (e.g., Dominik et al. 2012, 2013, 2015; de Mink & Belczynski 2015; Mapelli & Giacobbo 2018; Chu et al. 2022), such as Illustris-TNG (Pillepich et al. 2018) and EDGES (Schaye et al. 2015), limited by their small boxsize, normally $\sim 300\text{Mpc}$, while ignoring the potential effect of cosmic variance in our local universe. This **choice** may lead to a bias to the merger rate density evolution estimation and therefore the detection rate of BNS mergers, especially in the O2 run of LIGO-Virgo-KAGRA (hereafter LVK) GW detector network (Abbott et al. 2019b), for its small angle-averaged BNS detection range ($\sim 96\text{Mpc}$ for the LIGO-Livingston and 80Mpc for the LIGO-Hanford).

In this paper, we take the advantage of the large boxsize of the Millennium Simulation combined with the semi-analytic galaxy formation model GABE, and the parameterized population BSE model of our previous work to examine how much effect will the cosmic variance introduce on the estimation of merger rate density of BNS mergers. This paper is organized as follows. In Section 2, we briefly introduce the semi-analytic galaxy formation model GABE and the key parameters of BSE models. In Section 3, we present main results. Discussions and conclusions are given in Section 4. Throughout the paper, we adopt the cosmological parameters as $(h_0, \Omega_m, \Omega_\Lambda) = (0.68, 0.31, 0.69)$ (Aghanim et al. 2020).

2. SIMULATION RECIPES

The semi-analytical galaxy formation model GABE and N-body numerical simulation Millennium (e.g., Springel et al. 2005; Jiang et al. 2019) is adopted to estimate the cosmic merger rate density evolution of BNSs. The GABE model considers several important physical processes of galaxy formation, including the cosmic reionization, gas cooling with background radiation, star formation, supernova feedback, black hole growth, AGN feedback, and bar formation. As for the hierarchical growth of structure formation under the standard cold dark matter model, the tidal and ram-pressure stripping of hot gas, dynamical fraction, black hole growth and

star bursts in mergers and bulge formation are taken into account. More detailed description about the galaxy formation and evolution in GABE can be seen in Jiang et al. (2019).

The simulation box size is 685Mpc and the mass resolution of dark matter is $1.2 \times 10^9 M_\odot$, which allows us to generate a complete galaxy catalogue for galaxies more massive than $10^8 M_\odot$. We discrete the full box into 216 and 27 sub-boxes with boxsize of 100Mpc and 200Mpc respectively, which is about the twice the length of the comoving distance of the observed GW170817 ($\sim 50\text{Mpc}$) and O2 BNS observation horizon ($\sim 90\text{Mpc}$). Note that we do not consider the length scale of O3-O4a run (Abbott et al. 2021, 2023), for their large observation horizon, i.e., $\sim 150 - 200\text{Mpc}$. In such a scale, the cosmic variance is small enough for one to neglect its impact.

The merger rate density evolution of BNSs are mainly dependent on the metallicity and SFR density distribution across the universe, however, the dependency on metallicity is relatively weak. Therefore, the diversity of detection rate of BNS among those sub-boxes is due to the difference of galaxy-formation history in different sub-boxes caused by cosmic variances. Then, for each sub-box, we calculate the evolution of metallicity and SFR for each galaxy through tracing back its formation history by finding out all the progenitors in the whole cosmic merger trees.

Figure 1 shows the metallicity Z (left panel) and SFR evolution (right panel) with redshift z_s obtained from the semi-analytical galaxy formation model GABE and Millennium simulation. The blue dotted-dashed lines show the global (or the median) results for both metallicity Z and SFR evolution, while the inner and outer shaded regions represent the scatter induced by the cosmic variance among 27 sub-boxes with $l_{\text{subbox}} = 200\text{Mpc}$ and 216 sub-boxes with $l_{\text{subbox}} = 100\text{Mpc}$, respectively. We note here that for metallicity, our result are slightly higher than those constrained by Belczynski et al. (2016), but almost the same as the results in Chu et al. (2022) obtained from EAGLE and Illustris-TNG. Moreover, one can see that the metallicity Z and its evolution do not affect much by the cosmic variance among different sub-boxes. However, for the SFR density, the cosmic variance can have a significant effect, for which the resulted SFR density may vary by a factor of $\sim 1.3 - 2$. The largest SFR produced in a subbox can be higher than that with the smallest SFR by a factor of more than 3. Though it is currently not clear how much of an effect cosmic variance can introduce to the SFR density within the local volume (Madau & Dickinson 2014), observation of galaxy cluster survey shows that

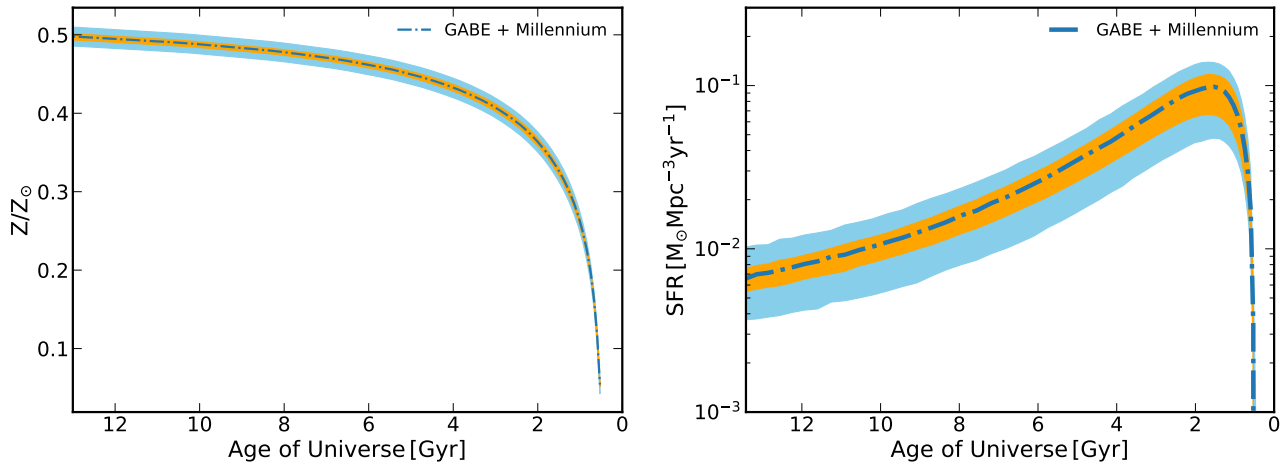


Figure 1. The metallicity evolution (left panel) and star formation rate SFR density evolution (right panel) with redshift z_s from the GABE semi-analytical galaxy formation model together with Millenium simulation. The blue dotted-dashed lines show the global results for both metallicity Z and SFR. The **inner orange shaded** area represents for the scatter induced by cosmic variance when $N_{\text{subbox}} = 27$ and correspondingly $l_{\text{subbox}} = 200\text{Mpc}$, while for **outer blue shaded** area represents the scatter when $N_{\text{subbox}} = 216$ and correspondingly $l_{\text{subbox}} = 100\text{Mpc}$.

Table 1. Model parameters of BSE models adopted, i.e., **$\alpha 10.\text{kb}\beta 0.9$** , **$\alpha 1.\text{kb}\beta 0.9$** and **$\gamma 1.5\text{kb}\beta 0.9$** . Here the 1st column α/γ represent parameters of the α/γ formalism of the common envelope ejection process respectively. The 2nd column σ_k is the dispersion of the natal kick distribution, which is assumed to be Maxwellian and bimodal, with $\sigma_k = 190\text{km s}^{-1}$ and 30km s^{-1} , respectively. The third column β represents the ratio of post-supernova to pre-supernova total system masses, which is set to be 0.9 across these three models. More details about the BSE model can be seen in [Chu et al. \(2022\)](#).

Model	α / γ	$\sigma_k(\text{km s}^{-1})$	β
$\alpha 10.\text{kb}\beta 0.9$	10	190/30	0.9
$\alpha 1.\text{kb}\beta 0.9$	1.0	190/30	0.9
$\gamma 1.5\text{kb}\beta 0.9$	1.5	190/30	0.9

there should be an underdensity in the matter distribution of about $\sim -30 \pm 15\%$ in a region with a radius of about 100Mpc ([Böhringer et al. 2020](#)). This may hint that the SFR density in local volume may be smaller than the average across the universe. Later, we shall see that the the cosmic variance affect the merger rate density of BNS mergers mainly via the scatter of SFR density.

We adopt the parameterized population models proposed in [Chu et al. \(2022\)](#) to mock the binary stellar evolution, including **$\alpha 10.\text{kb}\beta 0.9$** , **$\alpha 1.\text{kb}\beta 0.9$** and **$\gamma 1.5\text{kb}\beta 0.9$** . Among these models, the impacts of the common-envelope phase, natal kick, mass ejection during the secondary SN explosion, and metallicity are taken into account. The main differences between these three models are the choice of common-envelope descrip-

tion and the settings of model parameters. Here α and γ denote for the conserved energy and conserved angular momentum description in the mass-transfer process of common-envelope respectively. In our previous work, [Chu et al. \(2022\)](#) found that these three models rank the first three in the consistency check with the galactic BNS observations, by utilizing the Bayes factor methods. The key model parameters are listed in [Table 1](#) and more details about can be seen in [Chu et al. \(2022\)](#).

To reduce the cost of computing time, we do not implement the full BSE code into the GABE model together with Millenium simulation for each sub-box, but rather apply the N_{cor} description as discussed in [Mapelli & Giacobbo \(2018\)](#) to estimate the merger rate density evolution of BNSs $R^i(z_s)$ in the i -th discrete sub-box as

$$R^i(z_s) = \int dt_d P_t(t_d) f_b \text{SFR}^i(z_b) \times N_{\text{cor}}(Z^i(z_b)), \quad (1)$$

where f_b denotes the binary formation efficiency (normally $f_b = 0.5$), $\text{SFR}^i(z_b)$ is the star-formation rate density at the binary formation redshift z_b (or time t_b) in the i -th sub-box, and N_{cor} is the number of merging BNSs per unit mass in the i -th sub-box, which is directly related to the star metallicity $Z^i(z_b)$ at z_b . The term $t_d(z_b) = \int_{z_s}^{z_b} \left| \frac{dt}{dz} \right| dz$ denotes the time delay of a BNS merger from its progenitor binary star formation time and $P_t(t_d)$ is its probability distribution, ranging from 10Myr to a Hubble time t_H . Here we argue that the above estimation based on this simplified description is solid for N_{cor} is only related to the metallicity Z and different BSE models. [Figure 2](#) shows the dependence of N_{cor} as function of the binary progenitor's metallicity Z simulated by [Chu et al. \(2022\)](#). As seen

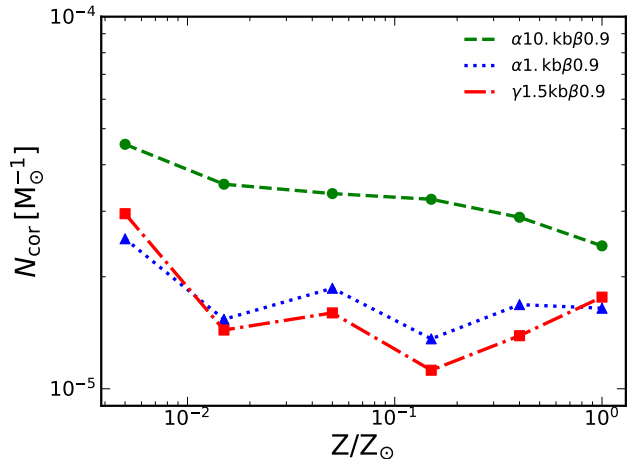


Figure 2. The relationship between number of merging BNSs per unit mass (N_{cor}) and the binary progenitor's metallicity (Z) simulated in [Chu et al. \(2022\)](#). The green dashed, blue dotted, and red dotted-dashed lines show the results of different parameterized population models, i.e., $\alpha 10.\text{kb}/0.9$, $\alpha 1.\text{kb}/0.9$ and $\gamma 1.5\text{kb}/0.9$, respectively.

from this figure that the value of N_{cor} can vary by a factor of 1 – 2 considering of different metallicities in different BSE models. This is due to the small mass range of NSs, regardless of whether it is formed through iron core-collapse or electron-capture SNe.

3. RESULTS

We obtain the the merger rate density evolution R^i of the BNS mergers in each sub-box as well as the global one from the whole box of Millennium simulation by integrating Equation (1) over all the snapshots of our cosmological simulation, i.e., $z_s \sim 0 - 10$ for 64 snapshots. Figure 3 shows the results of the merger rate density and its evolution by adopting the BSE model $\alpha 10.\text{kb}/0.9$. As seen from this figure, despite the slight bias of the median value ($R(z_s = 0) \sim 279 \text{Gpc}^{-3}\text{yr}^{-1}$ in our simulation), there is variation on $R(z_s)$ across the sub-boxes due to the cosmic variance. For example at the same redshift, the largest R is almost twice the value of the smallest R assuming $l_{\text{subbox}} = 100 \text{Mpc}$, for the SFR density in this sub-box is much higher.

To quantify the effect of cosmic variance on the merger rate density and the detection rate, we define the relative variance of a random variable X with cumulative probability distribution $P(X)$ by the following expression:

$$\frac{\sigma_X}{X} = \frac{X(P(X) = 0.84) - X(P(X) = 0.16)}{2X(P(X) = 0.5)}. \quad (2)$$

Figure 4 further plots the evolution of the relative variance σ_R/R with redshift z_s for these three models, assuming the sub-box size to be 100 Mpc (top panel) and

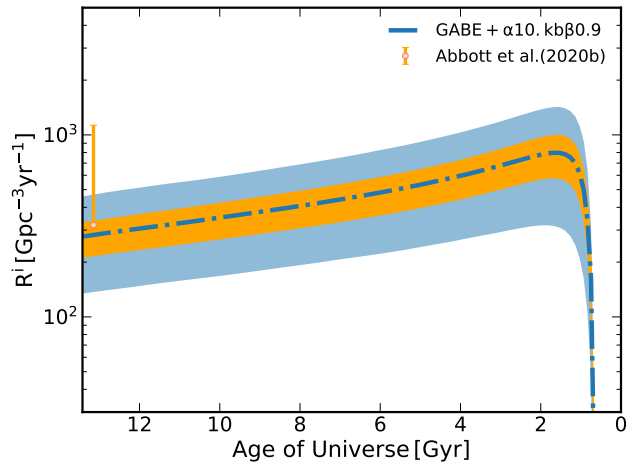


Figure 3. The comoving merger rate density evolution of BNS mergers R^i as a function of the age of universe obtained by adopting the $\alpha 10.\text{kb}/0.9$ BSE model. The blue dotted-dashed line shows the global results obtained by using the whole simulation box of Millennium simulation, and the inner orange and outer blue shaded regions show the scatter of R^i induced by the cosmic variance among the 27 and 216 discrete sub-boxes with size of $l_{\text{subbox}} = 100 \text{Mpc}$ and 200Mpc , respectively. The orange dot with error bar marks the local merger rate density obtained from the GW detections of the two BNS mergers (GW170817 and GW190425) ([Abbott et al. 2020](#)), i.e., $R(z_s = 0) \sim 320_{-240}^{+490} \text{Gpc}^{-3} \text{yr}^{-1}$.

200 Mpc (bottom panel), respectively. As seen from this figure, the larger the sub-box size, the higher the relative variance at a given redshift. For example, the local relative variance σ_R/R is about $\sim 12.0\%$ and $\sim 23.5\%$ for $l_{\text{subbox}} \sim 100 \text{Mpc}$ (top panel) and 200Mpc , respectively. This is easy to understand for the inhomogeneity of star formation decreases with the box size of the simulation, assuming a Gaussian random field. In addition, the evolution and scatter σ_R/R resulted from different models are quite similar, though the exact values of $R_{z_s}^i$ are different. This fact indicates that the estimation on σ_R/R can be viewed as reasonable and reliable, and their dependence on the choices of different binary population synthesis parameters is weak.

Moreover, the value of σ_R/R increases with increasing redshift, which can be mainly explained by the star formation history: the inhomogeneity of star formation is much higher, for voids are more common to exist at early times. As seen from Figure 4 that compared with the variance of SFR, σ_R/R is suppressed before $z_s \sim 2$ for different sub-box size case. This is mainly due to the time-delay from the binary star formation to their merger, which may flatten the difference of different boxes due to the integration effect.

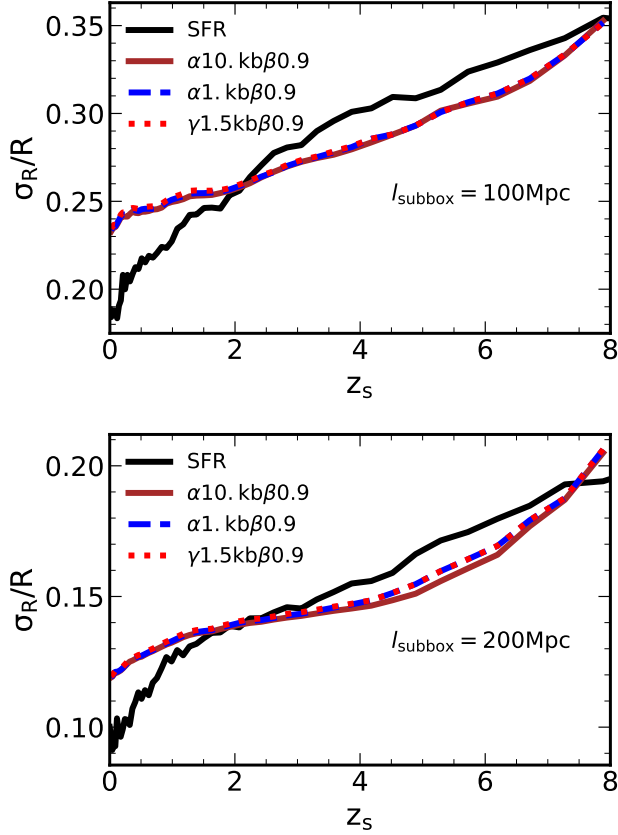


Figure 4. The evolution of the relative variance $\sigma(R)/R$ with redshift z_s with different sub-box length, i.e., $l_{\text{subbox}} = 100\text{Mpc}$ (upper panel) and $l_{\text{subbox}} = 200\text{Mpc}$ (bottom panel) respectively. The **brown solid**, **blue dashed** and **red dotted lines** show the results of different parameterized population models, i.e., $\alpha10.kb/0.9$, $\alpha1.kb/0.9$ and $\gamma1.5kb/0.9$ respectively. The black solid line shows the relative variance on the SFR.

With next-generation ground-based GW detectors, it is possible to localize BNS mergers within very small area. For example, with Cosmic Explorer (CE) networks, BNS mergers below $z_s \sim 0.2$ are expected to be localized within the sky area of $\Delta\Omega_s \sim 0.10\text{deg}^2$ and $\Delta d_L \sim 20\text{Mpc}$ (Zhao & Wen 2018). In such a small comoving volume, the impact of cosmic variance can be very large. We calculate the distribution of merger rate density with sub-box size of 40Mpc at $z_s = 0.2$ and the resulted distribution is shown in Figure 5. It can be seen that the relative variance σ_R/R is much larger, i.e., $\sim 55\%$. This result indicates that with future next-generation ground-based GW detectors, estimating the merger rate density of BNS in different sky areas may also provide useful information on the cosmic variance.

With the merger rate density evolution estimated by our ranked-first model $\alpha10.kb/0.9$, we may further check the variance on the detection rate of BNS merg-

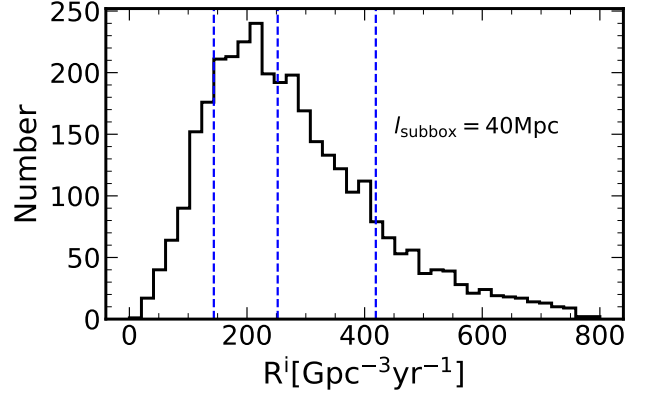


Figure 5. The distribution of BNS merger rate density of $15 \times 15 \times 15$ realization of sub-boxes, assuming $\alpha10.kb/0.9$ BSE model. The length of the sub-box is set to be 40Mpc, which corresponds to the localization precision of CE networks. The blue dashed lines from left to right show the 16%, 50%, 84% quantile of the distribution respectively.

ers in O2 run, σ_N/N , induced by the cosmic variance, following the standard Monte-Carlo procedure. We refer the readers to Zhao & Lu (2021) and Chen (2023) for details on the generation of mock BNS samples and their SNR calculation. We find that the variance on detection rate is about $\sim 13\%$ for detection threshold $\varrho_0 = 12$ and $\sim 9\%$ for $\varrho_0 = 8$. For GW observation runs post-O2, the variance is much smaller, less than $\lesssim 5\%$. During the writing procedure of this paper, we note that Morras & Garcia-Bellido (2024) also consider the effects of local cosmic inhomogeneities on the GW event rate, but simply assume the merger rate is proportional to the matter density. Using the peculiar velocities of galaxies from the CosmicFlows (CF) catalogs, they find that the cosmic variance effect on the compact binary coalescence event rate to be at most $\sim 6\%$, which is almost consistent with our results. Therefore, we conclude that the estimation of local merger rate density from the current observation of LVK is safe by ignoring the cosmic variance, for their very small impact on the detection rate. Here we also noticed that based on the observation of galaxy cluster survey, we find that the density of local volume (within 100Mpc radius) is $\sim 30\%$ under-dense from the average across the universe, which indicates that the detection rate of BNS mergers per comoving volume in our local universe may be smaller than the average value across the universe by a factor of $\sim 1-5\%$.

4. DISCUSSIONS AND CONCLUSIONS

In this work, we test the effect of cosmic variance on the merger rate density of binary neutron stars by adopting the galaxy formation model GABE based on the n-

body numerical simulation Millennium and the binary neutron star population synthesis model.

We find that for sub-box size of 100 Mpc and 200 Mpc, the relative variance of merger rate density σ_R/R at different redshift is about 0.23–0.35 and 0.13–0.20, respectively. With future powerful next-generation GW detectors, it is anticipated to detect $\sim 10^3$ – 10^4 BNS mergers. This indicate that one may constrain the cosmic variance via the estimation the BNS merger rate density in different sky areas. Moreover, we estimate the variance on the detection rate of BNS mergers, induced by the cosmic variance. We find that the relative variance of the detection rate is about $\sigma(N)/N \sim 0.05$ – 0.1 , which is small enough to not significantly impact the inferred merger rate density. As for future next-generation GW detectors, it is possible for one to localize BNS mergers into small sub-boxes. In such small comoving volume, the impact of cosmic variance on the merger rate density and therefore the detection number is much more significant. This offer a possible approach to constrain the cosmic variance by the spatial analysis of BNS mergers.

Note here that as the first estimation, there are many complexities we may need to further taken into account. For example, the absolute value of both σ_R/R and σ_N/N may vary slightly due to different settings in the semi-analytical simulations. Moreover, to reduce the cost of

computing, we did not run full population synthesis in each sub-box, but use simple description of BNS mergers by the SFR and metallicity to estimate the σ_R/R . This may also lead to slight difference on the results, though do not affect our main claim.

One may also conduct the parallel analysis to the stellar binary black hole mergers to check the effect of cosmic variance on their merger rate density. Besides, it is also possible to find a small sub-box very similar with our local observation in this model, which may provide interesting insights to the estimation of local merger rate density of compact binaries. We defer these aspects to future work.

ACKNOWLEDGEMENT

Zhiwei Chen thanks the daily-AstroCoffee organized in National Astronomical Observatories of China, and the speakers and audiences therein for their helpful discussions. This work is partly supported by the Strategic Priority Research Program of the Chinese Academy of Sciences (Grant no. XDB0550300), the National Natural Science Foundation of China (Grant nos. 12273050, 11991052), and the National Key Program for Science and Technology Research and Development (Grant nos. 2020YFC2201400 and 2022YFC2205201).

REFERENCES

- Abbott, B. P., Abbott, R., Abbott, T. D., et al. 2017a, *ApJL*, 848, L12, doi: [10.3847/2041-8213/aa91c9](https://doi.org/10.3847/2041-8213/aa91c9)
- . 2017b, *ApJL*, 848, L13, doi: [10.3847/2041-8213/aa920c](https://doi.org/10.3847/2041-8213/aa920c)
- . 2019a, *Physical Review X*, 9, 011001, doi: [10.1103/PhysRevX.9.011001](https://doi.org/10.1103/PhysRevX.9.011001)
- . 2019b, *Physical Review X*, 9, 031040, doi: [10.1103/PhysRevX.9.031040](https://doi.org/10.1103/PhysRevX.9.031040)
- Abbott, R., Abbott, T. D., Acernese, F., & Ackley, K. 2023, *Physical Review X*, 13, 041039, doi: [10.1103/PhysRevX.13.041039](https://doi.org/10.1103/PhysRevX.13.041039)
- Abbott, R., Abbott, T. D., Abraham, S., et al. 2020, *ApJL*, 896, L44, doi: [10.3847/2041-8213/ab960f](https://doi.org/10.3847/2041-8213/ab960f)
- . 2021, *Physical Review X*, 11, 021053, doi: [10.1103/PhysRevX.11.021053](https://doi.org/10.1103/PhysRevX.11.021053)
- Aghanim, N., Akrami, Y., Ashdown, M., et al. 2020, *A&A*, 641, A6, doi: [10.1051/0004-6361/201833910](https://doi.org/10.1051/0004-6361/201833910)
- Belczynski, K., Holz, D. E., Bulik, T., & O’Shaughnessy, R. 2016, *Nature*, 534, 512, doi: [10.1038/nature18322](https://doi.org/10.1038/nature18322)
- Böhringer, H., Chon, G., & Collins, C. A. 2020, *A&A*, 633, A19, doi: [10.1051/0004-6361/201936400](https://doi.org/10.1051/0004-6361/201936400)
- Chen, Z. 2023, *ApJ*, 953, 36, doi: [10.3847/1538-4357/ace045](https://doi.org/10.3847/1538-4357/ace045)
- Chu, Q., Yu, S., & Lu, Y. 2022, *MNRAS*, 509, 1557, doi: [10.1093/mnras/stab2882](https://doi.org/10.1093/mnras/stab2882)
- Coughlin, M. W., Dietrich, T., Margalit, B., & Metzger, B. D. 2019, *MNRAS*, 489, L91, doi: [10.1093/mnrasl/slz133](https://doi.org/10.1093/mnrasl/slz133)
- Coulter, D. A., Foley, R. J., Kilpatrick, C. D., et al. 2017, *Science*, 358, 1556, doi: [10.1126/science.aap9811](https://doi.org/10.1126/science.aap9811)
- de Mink, S. E., & Belczynski, K. 2015, *ApJ*, 814, 58, doi: [10.1088/0004-637X/814/1/58](https://doi.org/10.1088/0004-637X/814/1/58)
- Dobie, D., Kaplan, D. L., Murphy, T., et al. 2018, *ApJL*, 858, L15, doi: [10.3847/2041-8213/aac105](https://doi.org/10.3847/2041-8213/aac105)
- Dominik, M., Belczynski, K., Fryer, C., et al. 2012, *ApJ*, 759, 52, doi: [10.1088/0004-637X/759/1/52](https://doi.org/10.1088/0004-637X/759/1/52)
- . 2013, *ApJ*, 779, 72, doi: [10.1088/0004-637X/779/1/72](https://doi.org/10.1088/0004-637X/779/1/72)
- Dominik, M., Berti, E., O’Shaughnessy, R., et al. 2015, *ApJ*, 806, 263, doi: [10.1088/0004-637X/806/2/263](https://doi.org/10.1088/0004-637X/806/2/263)
- Gottlieb, O., Nakar, E., Piran, T., & Hotokezaka, K. 2018, *MNRAS*, 479, 588, doi: [10.1093/mnras/sty1462](https://doi.org/10.1093/mnras/sty1462)
- Jiang, Z., Wang, J., Gao, L., et al. 2019, *Research in Astronomy and Astrophysics*, 19, 151, doi: [10.1088/1674-4527/19/10/151](https://doi.org/10.1088/1674-4527/19/10/151)

- Madau, P., & Dickinson, M. 2014, *ARA&A*, 52, 415, doi: [10.1146/annurev-astro-081811-125615](https://doi.org/10.1146/annurev-astro-081811-125615)
- Mapelli, M., & Giacobbo, N. 2018, *MNRAS*, 479, 4391, doi: [10.1093/mnras/sty1613](https://doi.org/10.1093/mnras/sty1613)
- Morras, G., & Garcia-Bellido, J. 2024, arXiv e-prints, arXiv:2406.00691. <https://arxiv.org/abs/2406.00691>
- Pian, E., D'Avanzo, P., Benetti, S., et al. 2017, *Nature*, 551, 67, doi: [10.1038/nature24298](https://doi.org/10.1038/nature24298)
- Pillepich, A., Nelson, D., Hernquist, L., et al. 2018, *MNRAS*, 475, 648, doi: [10.1093/mnras/stx3112](https://doi.org/10.1093/mnras/stx3112)
- Schaye, J., Crain, R. A., Bower, R. G., et al. 2015, *MNRAS*, 446, 521, doi: [10.1093/mnras/stu2058](https://doi.org/10.1093/mnras/stu2058)
- Springel, V., White, S. D. M., Jenkins, A., et al. 2005, *Nature*, 435, 629, doi: [10.1038/nature03597](https://doi.org/10.1038/nature03597)
- The LIGO Scientific Collaboration, the Virgo Collaboration, the KAGRA Collaboration, et al. 2021, arXiv e-prints, arXiv:2111.03634. <https://arxiv.org/abs/2111.03634>
- Xie, X., Zrake, J., & MacFadyen, A. 2018, *ApJ*, 863, 58, doi: [10.3847/1538-4357/aac9c](https://doi.org/10.3847/1538-4357/aac9c)
- Zhao, W., & Wen, L. 2018, *PhRvD*, 97, 064031, doi: [10.1103/PhysRevD.97.064031](https://doi.org/10.1103/PhysRevD.97.064031)
- Zhao, Y., & Lu, Y. 2021, *MNRAS*, 500, 1421, doi: [10.1093/mnras/staa2707](https://doi.org/10.1093/mnras/staa2707)